

# Fluorescence diffuse tomography for detection of red fluorescent protein expressed tumors in small animals

Ilya V. Turchin  
Vladislav A. Kamensky  
Vladimir I. Plehanov  
Anna G. Orlova  
Mikhail S. Kleshnin  
Ilya I. Fiks

Institute of Applied Physics RAS  
46 Ulyanov Street  
603950 Nizhny Novgorod, Russia

Marina V. Shirmanova

Nizhny Novgorod State University  
23 Prospect Gagarina St.  
603950 Nizhny Novgorod, Russia

Irina G. Meerovich  
Lyaisan R. Arslanbaeva  
Viktoria V. Jerdeva  
Alexander P. Savitsky

A.N. Bach Institute of Biochemistry RAS  
33/2 Leninsky Prospekt St.  
190071 Moscow, Russia

**Abstract.** A fluorescence diffuse tomography (FDT) setup for monitoring tumor growth in small animals has been created. In this setup an animal is scanned in the transilluminative configuration by a single source and detector pair. To remove stray light in the detection system, we used a combination of interferometric and absorption filters. To reduce the scanning time, an experimental animal was scanned using the following algorithm: (1) large-step scanning to obtain a general view of the animal (source and detector move synchronously); (2) selection of the fluorescing region; and (3) small-step scanning of the selected region and different relative shifts between the source and detector to obtain sufficient information for 3D reconstruction. We created a reconstruction algorithm based on the Holder norm to estimate the fluorophore distribution. This algorithm converges to the solution with a minimum number of fluorescing zones. The use of tumor cell lines transfected with fluorescent proteins allowed us to conduct intravital monitoring studies. Cell lines of human melanomas Mel-P, Mel-Ibr, Mel-Kor, and human embryonic kidney HEK293 Phoenix were transfected with DsRed-Express and Turbo-RFP genes. The emission of red fluorescent proteins (RFPs) in the long-wave optical range permits detection of deep-seated tumors. *In vivo* experiments were conducted immediately after subcutaneous injection of fluorescing cells into small animals. © 2008 Society of Photo-Optical Instrumentation Engineers. [DOI: 10.1117/1.2953528]

Keywords: fluorescence diffuse tomography; whole-body imaging; fluorescent proteins; molecular imaging; algebraic reconstruction technique; Holder norm.

Paper 07420SSR received Oct. 9, 2007; revised manuscript received Mar. 7, 2008; accepted for publication Apr. 14, 2008; published online Aug. 25, 2008.

## 1 Introduction

Fluorescent imaging based on the specific marking of tumors is widely used in experimental oncology. Generally, fluorescent agents are selectively accumulated in cancer cells due to their chemical nature or through binding with specific proteins such as antibodies for tumor antigens. The possibility to introduce genes of a particular class of fluorophores—fluorescent proteins (FPs)—into cells enabled the development of a new method: genetic marking. The fluorescence ability of FPs persists for the whole life of a cancer cell and remains after cell division. As a result, it becomes possible to estimate tumor growth rate, to study the mechanism of carcinogenesis and metastasis formation, and to investigate the safety and efficacy of intervention using novel therapeutics.<sup>1–4</sup> Recently, a new group of FPs—red fluorescent proteins (RFPs)—was isolated, and they became useful as markers for whole-body biological imaging. The fluorescence spectrum of these proteins is in the relatively long-wave part of the spectrum (580 to 650 nm), a region that is promising for object

visualization at depths up to 1 to 2 cm with millimeter resolution.<sup>5–7</sup> Therefore, RFP-labeled tumors can be regarded as the most appropriate model for whole-body investigations.

Fluorescence tomography—time domain (TD), frequency domain (FD), and continuous wave (CW)—use reconstruction algorithms that account for the effects of diffuse light propagation in tissue.<sup>8–21</sup> Appropriate theoretical model of photon propagation in tissues with the corresponding mathematical inversion permits one to determine, with high resolution, the real boundaries of tumors located deep in animals. These techniques are used mainly to investigate the distribution of near-infrared fluorescent probes. Only a few works have been devoted to fluorescence diffuse tomography (FDT) with excitation in visible light.<sup>17–21</sup> Highly sensitive systems are required to detect fluorescent light at large depths (>5 to 7 mm) due to the high absorption rate of biological tissue in this spectral range. Photomultiplier tubes (PMTs) and cooled charge-coupled devices (CCD) are traditionally used for fluorescence detection. By employing a CCD, one can collect data from many source-detector positions in a relatively short time.<sup>13</sup> But a CCD with analogous sensitivity is

Address all correspondence to: Ilya V. Turchin, Institute of Applied Physics RAS, 46 Ulyanov Street, 603950 Nizhny Novgorod, Russia. Tel: 7 831 4164804; Fax: 7 831 4363792; E-mail: ilya@uifp.appl.sci-nnov.ru

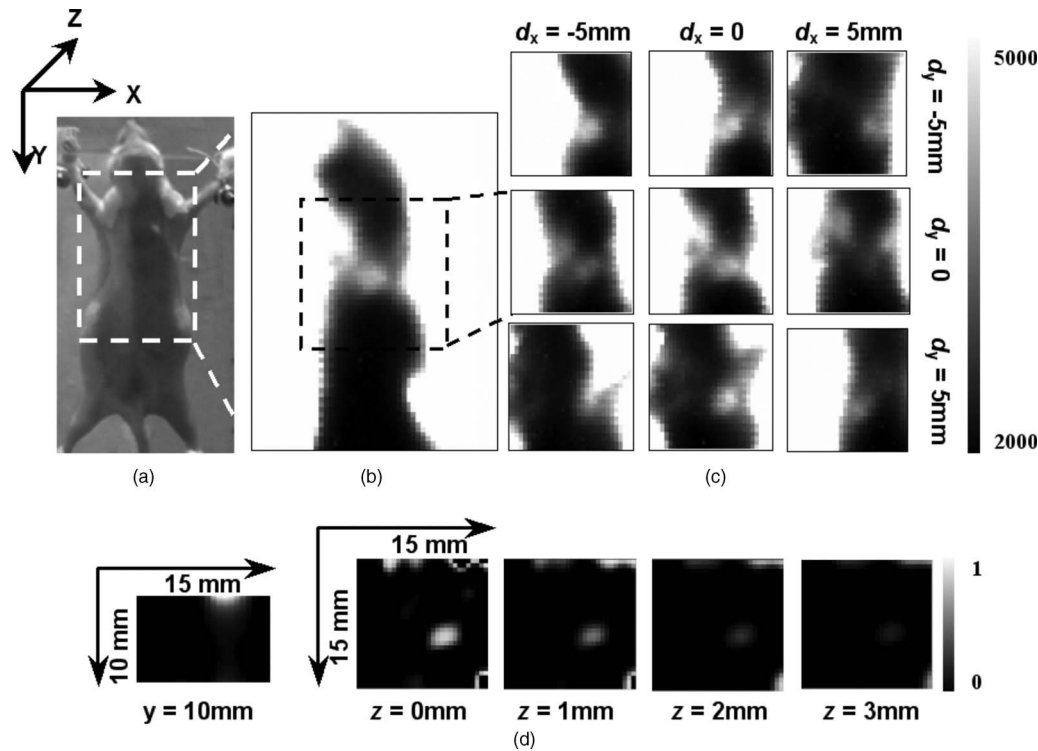


**Fig. 1** Algorithm of scanning an experimental animal (a) by FDT setup: obtaining a general view of the animal (b), and scanning of the selected fluorescing region with different shifts between source and detector (c) ( $d_x, d_y$ —shifts between source and detector in the scanning plain  $xy$ ). Reconstructed distribution of fluorophore concentration (d).

expensive and does not allow one to use modulated light. Moreover, the large data volume ( $10^5$  to  $10^8$  source-detector points) obtained with a CCD is usually merged into an array with smaller size for 3D reconstruction. The systems with multiple detectors coupled with fibers, which make contact with an experimental animal through an immersion liquid, are also well known.<sup>14</sup> These systems also have high acquisition rates; but they are complex, and the distance between their collecting fibers is fixed and does not allow for detailed scanning.

In our FDT setup, we used a single source-detector pair and a mechanical scanning system. This device is more time-consuming for animal scanning but has a lower cost than the systems described above. Programmable source and detector positions enable one to set the optimal law of source-detector travel. To reduce the time of investigation, an experimental animal was scanned using the following algorithm (Fig. 1): (1) large-step scanning to obtain a general view of the animal (source and detector move synchronously); (2) selection of the fluorescing region; and (3) small-step scanning of the selected region and different relative shifts between the source and detector to obtain sufficient information for 3-D reconstruction. To optimize the detailed scanning procedure, we chose scanning parameters (scanning area, scanning step sizes) according to the recommendations given in Ref. 22. The detector was set as close as possible to the surface of the mouse. This enabled us to collect fluorescent light with a higher numerical aperture (NA), thus providing a higher signal. The detector consisted of diaphragms, filters, an optical beam, and a PMT module. The sensitivity of such a system is

also determined by the optical density (OD) of the optical filters. The OD of interferometric filters is limited to the value of 5. Using a combination of interferometric and absorption filters allowed us to achieve an OD value of 6. We applied low-frequency modulation to increase the signal-to-noise ratio. Plane geometry was used in our FDT setup to minimize the thickness of the transilluminating tissue. Thus, the decay of the light propagated through the mouse was minimized.

The algebraic reconstruction technique (ART) is a powerful method for reconstruction of the fluorophore concentration.<sup>13,23,24</sup> This algorithm provides good transversal resolution but poor in-depth resolution for plane geometry if no information about transmitted excitation light has been obtained. This is the result of the ART's instability in relation to the errors in the kernel of the solving equation [errors of matrix  $\mathbf{A}$  in the system of linear equations Eq. (3)]. In this paper we suggest the reconstruction algorithm with the Holder norm to minimize discrepancy. This algorithm decreases the number of voxels with a nonzero fluorophore concentration in the reconstructing distribution of the fluorophore, thus decreasing the "freedom" of the solution. Hence, the result of the reconstruction appears "nearer" to the true distribution compared with the ART.

We performed a series of model and *in vivo* experiments with nude mice after injecting them with Turbo-RFP and DsRed-Express-HEK293 cells. The ability of the FDT method to detect fluorescent-marked cells in an animal body and to conduct monitoring experiments was demonstrated. Three-dimensional tumor reconstruction in the model and *in vivo* experiments was performed.

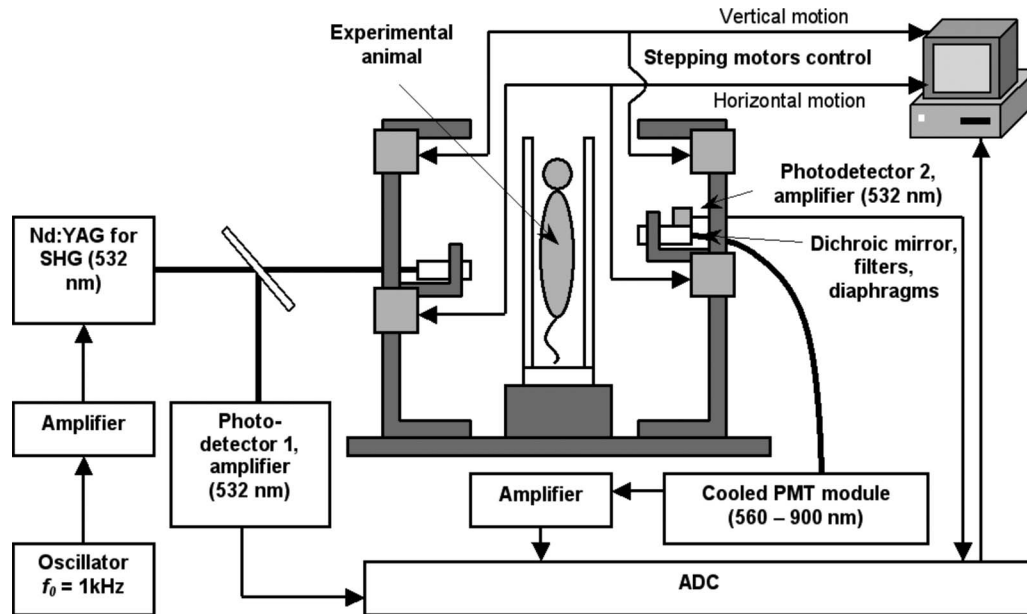


Fig. 2 Schematic of the FDT experimental setup.

## 2 Materials and Methods

### 2.1 FDT Experimental Setup

Experiments with FDT were performed using FPs from the RFP family: DsRed2, DsRed-Express, and Turbo-RFP. These proteins have similar positions of fluorescence maximums in the red-orange spectral region and are suitable for whole-body imaging. Low-frequency modulated light ( $f_0 = 1$  kHz) from a Nd:YAG laser with second-harmonic generation at a 532-nm wavelength (ATC-Semiconductor devices, Russia), which is close to the absorption maximum of RFPs, was used in the experimental setup (Figs. 2 and 3). The power on the investigated object was 20 mW, the beam diameter was 0.5 mm, the aperture of the detector was 0.5 mm, and the NA of the detector was 0.22. A dichroic mirror was placed behind the input diaphragm to separate emission (540 to 650 nm) and excitation (532 nm) light transmitted through the experimental animal. The transmitted excitation light was detected by an Edmund Optics photodetector (photodetector 2 in Fig. 2). To detect fluorescent light, we used a high-sensitivity cooled PMT Hamamatsu H7422-20. The suppression of excitation

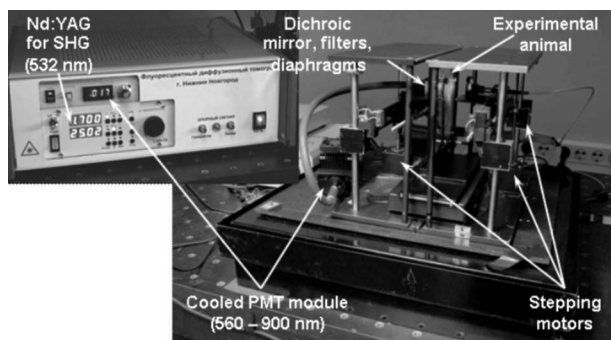


Fig. 3 FDT experimental setup created at the Institute of Applied Physics, Russia.

spectra at the detector input of the PMT module was approximately 6 ODs. This value was achieved by using the interferometric filter (Chroma Technology, USA) in combination with the absorption filter. The absorption filter was installed between the interferometric filter and the detector. This installation prevented possible fluorescence of the absorption filter. The interferometric filter had a sharper edge transmittance curve than the absorption filter, so, the short-wavelength part of the fluorescence spectrum was suppressed stronger than the long-wavelength part. But in the case of an RFP, the short-wavelength part of the fluorescence spectrum has a much higher absorption coefficient and can be neglected.

During the experiment, an animal was placed vertically in a container consisting of a supporting plate and a covering glass plate that was slightly pressed to fix the animal. The distance between the plates was about 1 cm. Synchronous scanning of the object in the transilluminative configuration was provided by a single pair of a source and a detector set in motion by stepping motors (Intelligent Motion Systems, Korea).

One source-detector measurement took about 50 ms. Obtaining a general view of the animal with large steps [when the source and detector move synchronously, Fig. 1(b)] took about 2 to 3 minutes, and detailed scanning of the fluorescent region [Fig. 1(c)] for 3D reconstruction took about 20 minutes.

### 2.2 Reconstruction of the Fluorophore Concentration

Fluorescent signal  $P$  can be written in the following form:<sup>8,25</sup>

$$P(\mathbf{r}_d, \mathbf{r}_s) = \int \Sigma(\mathbf{r}) G(|\mathbf{r} - \mathbf{r}_s|, |\mathbf{r}_d - \mathbf{r}|) d^3\mathbf{r}, \quad (1)$$

where  $\mathbf{r}_d$  and  $\mathbf{r}_s$  are detector and source coordinates,  $\Sigma(\mathbf{r})$  is the fluorophore distribution (the product of the absorption cross-section and the fluorescence quantum yield), and  $G$  is a

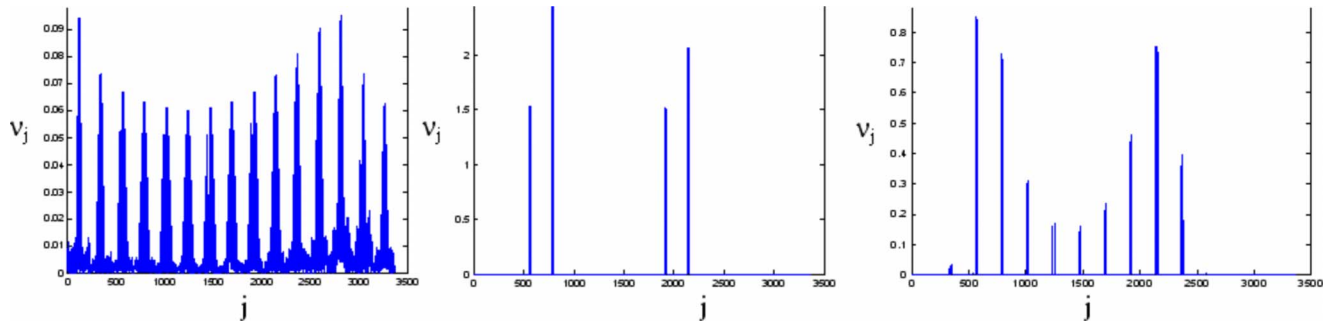


Fig. 4 Typical solving vectors  $\mathbf{v}$  for reconstruction algorithm based on the Holder norm with  $\xi=2$ ,  $\xi=10^{-5}$ , and  $\xi=0$  (corresponding to the fluorophore distribution shown in Fig. 5).

Green's function that defines the fluorescence response measured at the distance  $|\mathbf{r}_d - \mathbf{r}|$  from a point fluorophore located at the distance  $|\mathbf{r} - \mathbf{r}_s|$  from the source. In the diffusion approximation of the radiative transport equation,  $G$  can be written in the following form:<sup>8,26</sup>

$$G(R_1, R_2) = C \frac{\exp(-\alpha_1 R_1 - \alpha_2 R_2)}{R_1 R_2}. \quad (2)$$

Here,  $\alpha_1$  and  $\alpha_2$  are diffusion attenuation coefficients for excitation and fluorescent light, respectively, and  $C$  accounts for the boundaries. Boundary conditions are the following:<sup>24</sup>

$$\alpha(R_1, R_2) \frac{\partial}{\partial \eta} G(R_1, R_2) + G(R_1, R_2) = 0,$$

where  $\partial/\partial \eta$  is the derivative in the direction of the outer normal to the surface, and  $\alpha$  is the arbitrary function. This condition is determined by the method of images described in Refs. 9 and 27.

To solve the inverse task for Eq. (1), one can write it in discrete form:<sup>13</sup>

$$\begin{aligned} \Sigma(\mathbf{r}) \rightarrow v_j P(\mathbf{r}_d, \mathbf{r}_s) \rightarrow P_i G(|\mathbf{r} - \mathbf{r}_s|, |\mathbf{r}_d - \mathbf{r}|) \rightarrow A_{ij} \\ A\mathbf{v} = \mathbf{p}. \end{aligned} \quad (3)$$

Here,  $j = 1..N$ ,  $N = N_x N_y N_z$  is the number of voxels of unknown fluorophore distribution (where  $N_x$ ,  $N_y$ , and  $N_z$  are the number of voxels in the  $X$ ,  $Y$ , and  $Z$  directions), and  $i = 1..M$  is the projection number (the number of raw data for the source and detector  $r_{si}$  and  $r_{di}$  coordinates). Each voxel with  $(x, y, z)$  coordinates can be numbered as following:

$$j = (x - 1)N_y N_z + (y - 1)N_z + z.$$

The main features of matrix  $\mathbf{A}$  are well known: big size (usually  $N > 10^4$ ), bad conditionality (about  $10^{17}$ ), no zero elements, and positively defined. Unfortunately, such methods as the Gaussian algorithm, the inversion of matrix  $\mathbf{A}$ , the determination of eigenvectors, etc., are not applicable for solving the inverse task of Eq. (3). Therefore, iteration algorithms are usually used to solve Eq. (3). Traditionally, Eq. (3) has been solved by the ART or its modifications (such as multiplicative algebraic reconstruction technique, simultaneous algebraic reconstruction technique, etc.).<sup>13,23,24</sup> As was men-

tioned above, this algorithm has poor in-depth resolution for a planar configuration. To improve the in-depth resolution, we suggest another algorithm based on the Holder norm. The Holder norm of arbitrary vector  $\mathbf{v}$  can be written as follows:

$$\|\mathbf{v}\|_{\xi} = \left( \sum_{j=1}^N |v_j|^{\xi} \right)^{1/\xi}. \quad (4)$$

The main feature of this norm is: if  $\xi \rightarrow 0$ , then the value of  $\|\mathbf{v}\|_{\xi} \rightarrow N'$ , where  $N' \leq N$  is the number of nonzero elements of vector  $\mathbf{n}$ . In other words, by minimizing Eq. (4) among all the solution sets of Eq. (3), we obtain the minimum number of reconstruction "peaks" of vector  $\mathbf{n}$ . It corresponds to the minimum number of zones with a nonzero fluorophore concentration. The special case  $\xi=2$  corresponds to the ART. An example of typical solving vectors  $\mathbf{v}$  for  $\xi=2$ ,  $\xi=10^{-5}$ , and  $\xi=0$  is shown in Fig. 4. As shown in Fig. 4, the lower the value of  $\xi$ , the fewer peaks there are in the solving vectors.

The iteration procedure for an algorithm with the minimum Holder norm [Eq. (4)] and  $\xi \rightarrow 0$  has the following form:

$$\mathbf{v}^{(k+1)} = D_0^{-1} [\mathbf{v}^{(k)}] \mathbf{A}^T \{ \mathbf{A} D_0^{-1} [\mathbf{v}^{(k)}] \mathbf{A}^T \}^{-1} \mathbf{p}, \quad (5)$$

where  $D_{\xi}(\mathbf{v}) = \text{diag}[(v_j^2 + \epsilon)^{\xi/2 - 1}]$  is a diagonal matrix, and  $\epsilon$  is a small positive number (usually  $10^{-6}$  to  $10^{-9}$ ). The derivation of this formula is described in the Appendix. A comparison of the reconstruction results using the ART and the Holder norm is presented in Fig. 5. As shown in Fig. 5, the reconstruction by the ART [Fig. 5(b)] has rather poor in-depth resolution than the reconstruction using the Holder norm [Figs. 5(c) and 5(d)]. By decreasing the Holder norm exponent factor  $\xi$ , we decrease the number of voxels with a nonzero fluorophore concentration in the reconstructed array, thus decreasing the "freedom" of the solution. Hence, the result of the reconstruction appears "nearer" to the true distribution for small values of  $\xi$ . This corresponds to a better spatial resolution. The number of iterations for the algorithm convergence does not depend too much on the factor  $\xi$ , except in the special case  $\xi=2$  when the algorithm consists of a single iteration. The value of  $\xi$  regulates the influence of errors in Eq. (3) (in the left part as well as in the right part) on the solution. We recommend choosing a  $\xi$  value in the range of  $0.2 \leq \xi \leq 1.5$ , because if  $\xi$  is less than 0.2, the reconstruction is not robust; if  $\xi$  is greater than 1.5, there is no advantage over the ART.

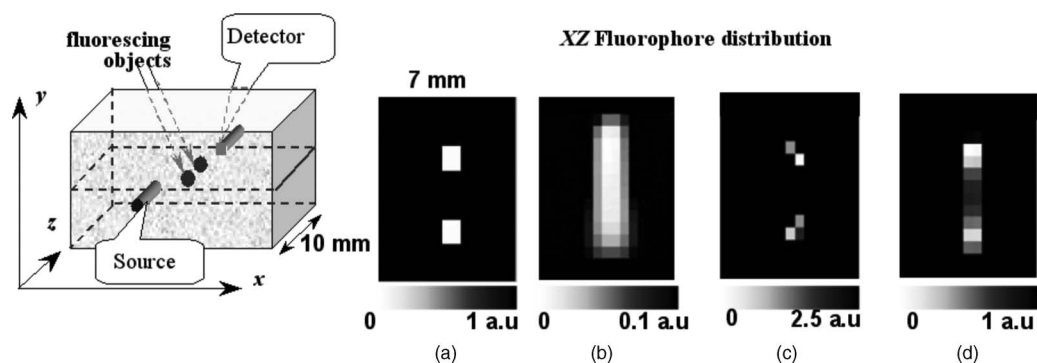


**Fig. 5** Numerical experiment of reconstruction of two fluorescent inclusions in scattering medium: (a) initial distribution of the fluorophore concentration in the XZ plane; (b) reconstruction of the fluorophore distribution using the ART; (c) and (d) reconstruction of the fluorophore distribution based on the Holder norm with  $\xi=10^{-5}$  and  $\xi=1$ , respectively.

We should note that this reconstruction method has two significant disadvantages: (1) it must allocate memory for auxiliary data, and (2) it is more time consuming than the ART. For example, the computational time on a four-core, 2.2-GHz processor is about two hours for 1500 source-detector measurements and 3500 voxels in the reconstructing volume.

### 2.3 Fluorescent Proteins

The properties of the FPs used in this work are shown in Table 1. The proteins have similar positions of fluorescence maximums in the red-orange spectral region. Fluorescent protein DsRed-Express has better properties than RFP DsRed2. DsRed-Express is a rapidly maturing variant of the *Disco-soma* sp. RFP (DsRed). It contains nine amino acid substitutions that enhance its solubility and reduce its green emission. DsRed-Express displays a reduced tendency to aggregate and hence a lower toxicity to cells. TurboRFP is a novel RFP derived from anemone *Entacmaea quadricolor*. Possessing high photo and pH stability, TurboRFP has a quantum yield and an extinction coefficient higher than those of DsRed2, and it is about twice as bright as DsRed2. The fast maturation of DsRed-Express and TurboRFP makes them clearly detectable

**Table 1** Properties of Turbo-RFP, DsRed2, and DsRed-Express (see www.evrogen.com and Refs. 28–31).

Characteristics	Turbo-RFP	DsRed2	DsRed-Express
Excitation max (nm)	553	563	557
Emission max (nm)	574	582	579
Quantum yield	0.67	0.55	0.4
Extinction coefficient (M <sup>-1</sup> cm <sup>-1</sup> )	92 000	43 800	30 100
Brightness	61.6	24.1(35.8)	12.6
Structure	dimer	tetramer	tetramer
Detection in mammalian cells (hrs after transfection)	8–12	36–48	8–12

in mammalian cells as early as 8 to 12 hours after transfection.<sup>28</sup>

Human melanoma cell lines were received from the Institute of Experimental Diagnostics and Therapy of Tumors at the N. N. Blokhin Russian Cancer Research Center. The plasmids pDsRed2-C1, pDsRed-Express-C1 (Clontech, USA), and Turbo-RFP-C (Eurogen, Russia) were used for transfection. We obtained cell lines of human melanoma Mel-P, Mel-Ibr, Mel-Kor, and human embryonic kidney HEK293 Phoenix, which express the RFPs. The fluorescence intensity of the transfected cells substantially exceeded the intensity of the initial nontransfected cells. It was demonstrated that transfection did not change the tumor cell growth rate or morphology. Examples of microphotographies of cells and their fluorescence spectra at different time points after transfection are shown in Fig. 6.

## 3 Results

A series of model and *in vivo* experiments were conducted using the experimental FDT setup described above.

### 3.1 Model Experiment

The scheme of the model experiment is shown in Fig. 7 (left side): a quartz box  $50 \times 27 \times 19$  mm (W  $\times$  H  $\times$  D) containing a water solution of intralipid and Indian ink. The absorption coefficient of the bulk medium was  $\mu_a=0.1$  cm<sup>-1</sup>, and the reduced scattering coefficient was  $\mu'_s=4$  cm<sup>-1</sup>. A glass capsule with an internal diameter of 2.5 mm containing DsRed2 with a concentration of  $10^{-6}$  M/l was placed in the center of the box. The bulk solution was added to the DsRed2 to provide the same scattering parameters in the capsule as those in the surrounding medium. The average absorption coefficient in biotissue is higher than that in the model medium, but the thickness of the quartz box was higher than the thickness of the experimental animal. In this experiment we simulated the same attenuation of light propagated through the whole model medium as that in the *in vivo* experiment. It is more convenient in a thicker model medium to simulate small (on the scale of the whole medium) fluorescent tumors located at different depths. The results of the 3-D reconstruction of the fluorophore concentration in the XY and XZ planes are shown in Fig. 7 (right). The figure shows that the results of the re-

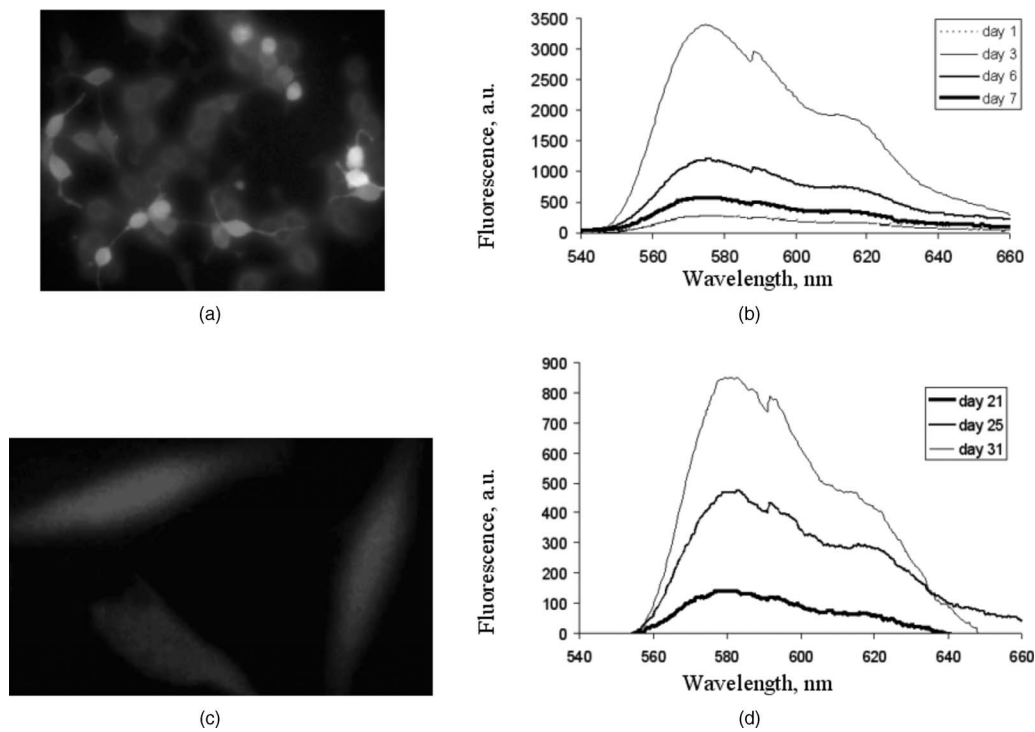


**Fig. 6** (a) Microphotography, and (b) fluorescence spectra of stably fluorescing Mel-Kor-DsRed-Express cells. (c) Microphotography, and (d) fluorescence spectra of transitory transfected HEK293-Turbo-RFP cells.

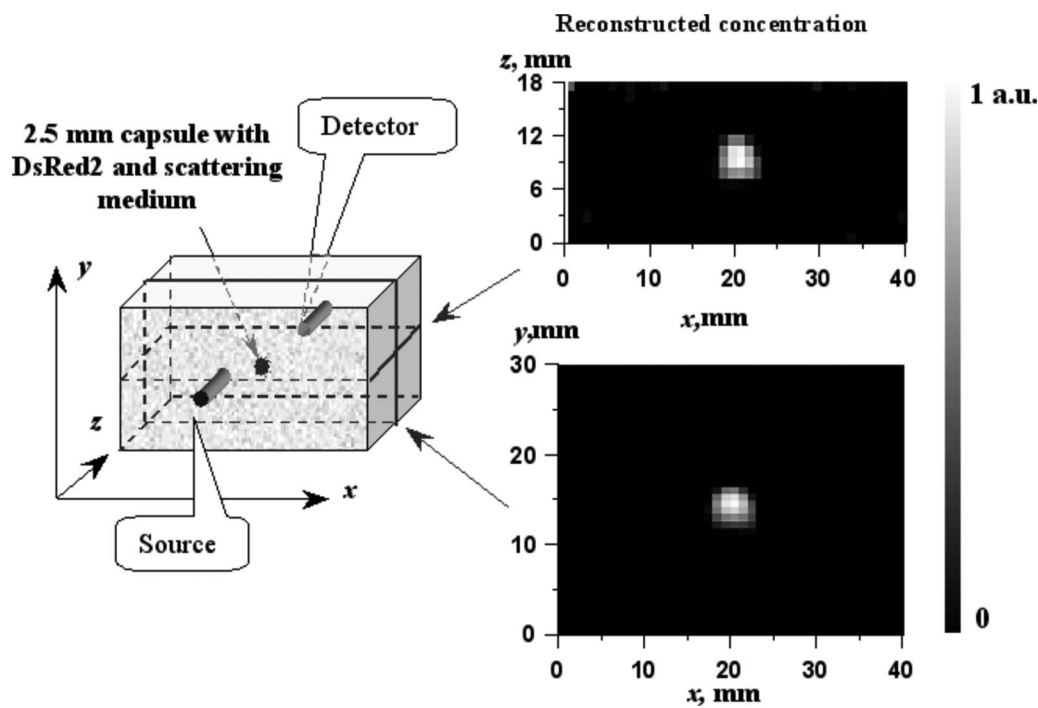


**Fig. 7** Results of 3-D reconstruction of the fluorophore concentration in the model medium: a glass capsule containing DsRed2 suspension was placed in a quartz box  $50 \times 27 \times 19$  mm (W $\times$ H $\times$ D) in size containing a water solution of intralipid and Indian ink. Bulk scattering medium:  $\mu_a = 0.1 \text{ cm}^{-1}$ ,  $\mu_s' = 4 \text{ cm}^{-1}$ .

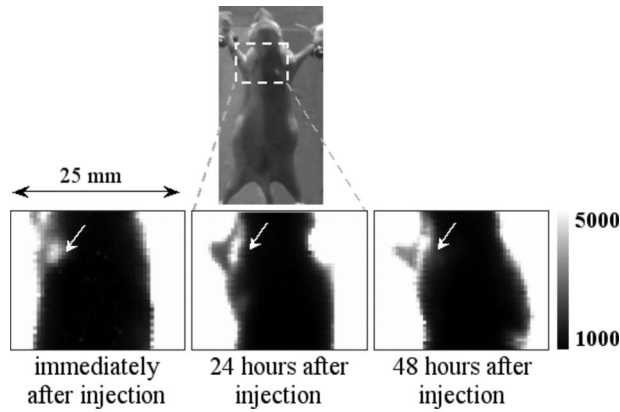


**Fig. 8** Fluorescent images obtained in a transillumination configuration of source and detector of a nude mouse after injection of HEK293-Turbo-RFP cells. The images were obtained (from left to right) immediately after injection, 24 hours later, and 48 hours later. Number of cells: 1.7 million; suspension volume: 50  $\mu\text{l}$ .

construction are in good agreement with the initial fluorophore distribution.

### 3.2 In Vivo Experiments

Whole-body FDT experiments were performed using HEK293 cells transfected with RFPs. A suspension of fluorescing HEK293 cells was injected subcutaneously into a female 12-week old nude mouse. Before the experiment, the anaesthetized animal was fixed on the supporting plate of the container. A 50- $\mu\text{l}$  suspension containing 1.7 million of cells was used in our experiments with Turbo-RFP. The FDT data of the mouse were obtained before the injection of the HEK293-Turbo-RFP suspension, then immediately after the

injection, and 24 and 48 hours later (Fig. 8). The maximal intensity increase of the fluorescent signal was observed immediately after the injection. The results of subsequent imaging indicate a decrease of fluorescence intensity, possibly due to a redistribution of fluorescing cells near the region of injection. In the injection zone of the untransfected control HEK293 cells, no changes in fluorescence intensity were registered.

The results of 3-D reconstruction in our *in vivo* experiments are shown in Fig. 9. In this series of experiments, we used a 50- $\mu\text{l}$  suspension containing 50,000 HEK293-Turbo-RFP cells. As is clear from the results of the reconstruction, the concentration of the fluorophore is higher on the surface of the animal, namely in the injection area.

## 4 Discussion

The results of our experiments demonstrate the ability of the FDT method to detect fluorescence-marked cells in a small animal body, to perform 3-D tumor reconstruction, and to carry out monitoring experiments. These results may be used to investigate tumor growth and metastasis formation mechanisms, and to estimate therapeutic responses.

The fluorescence of stably transfected cell lines Mel-P, Mel-Ibr, and Mel-Kor can be detected for a rather long period after transfection. Utilization of these cells seems to be the most appropriate approach for long-term monitoring studies. Transitory transfected HEK293 cell lines fluoresce for only 7 days, though the fluorescence intensity of these cells exceeds that of transfected melanoma cells. Thus, we can use the less number of HEK293 than melanoma cells for a short-term *in vivo* experiment. In the present study, the 50,000 transfected HEK293 cells were a sufficient number for whole-body imaging. For long-time monitoring investigations, we

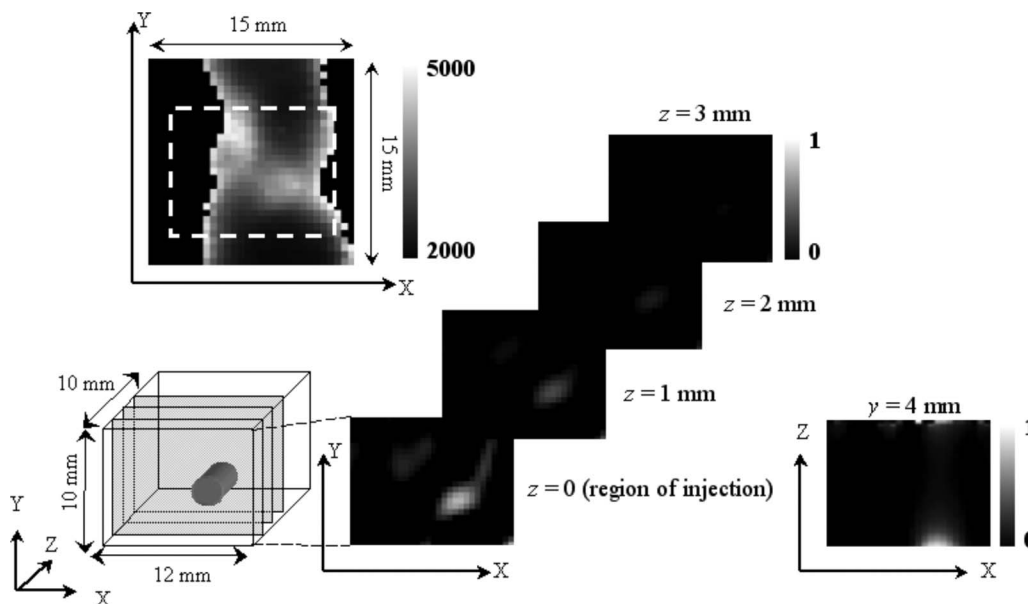


**Fig. 9** Results of the 3-D reconstruction of the fluorophore concentration after a hypodermic injection of suspension with 50,000 cells of HEK293-Turbo-RFP; the volume of injection was 50  $\mu\text{l}$ . The thickness of the object was 10 mm. In the upper left corner, the distribution of the fluorescent signal obtained by synchronous scanning of the source and detector is shown. The white dashed line shows the area of the 3-D reconstruction. From the bottom left corner to the upper right corner, the results of the 3-D reconstruction are given for four different depths:  $z=0$  (place of injection), 1, 2, and 3 mm.

plan to use stably transfected cell lines that do not lose their ability for FP expression for a long period.

The 3-D reconstruction in *in vivo* studies was performed only for the subcutaneous injection of fluorescing cells to simulate a tumor. The possibility of 3-D reconstruction on deeply located tumors was demonstrated only on the model medium.

In the described setup we used plane geometry, which allowed us to minimize the thickness of the biotissue. Thus, the decay of the light propagated through the mouse was less than that of cylindrical geometry.<sup>14</sup> In addition, the detection system in our FDT setup, based on a cooled PMT module with low-frequency modulation, had a very high sensitivity. However, 3-D reconstruction of a fluorophore concentration is more robust with cylindrical geometry than with plane geometry.

The use of the normalized Born approach in the reconstruction algorithm may significantly improve the quality of a reconstruction.<sup>32</sup> But detecting green light propagated through biotissue is complicated by the high intensity of light that is scattered in the supporting plate and propagated around an experimental animal. Moreover, the dynamic range of the “green” detector (detector 2 in Fig. 2) should be very high to detect the excitation light propagated through the experimental animal in areas of different thickness. By using an immersion liquid, the intensity of stray light will be decreased and the thickness of the transilluminating medium will be constant, so the detection of excitation light will be possible. Moreover, boundary conditions in this case were taken into account automatically. The use of an immersion liquid does increase the complexity of *in vivo* studies. In our opinion the most appropriate way to improve the quality of a reconstruction is to install an additional red light source and to detect red light propagated through the tissue.

The problem of using the normalization Born approach, connected with the detection of the excitation light, led us to update the ART method that we used for reconstruction of the fluorophore concentration in our first experiments. Using the described technique with the Holder norm is more time consuming than the ART, but it produces a higher-quality reconstruction. The described experimental setup yields a small data volume, but it is reasonable to use a reconstruction algorithm with greater computational complexity.

Another limiting factor for the detection of FP emission with low intensity is autofluorescence. This is not an acute problem if one works with nude mice. But even a small background can be a limiting factor for detecting small concentrations of fluorophore. The most effective way to overcome this limitation is to add spectral resolution measurements<sup>33</sup> and/or lifetime measurements using the frequency-domain technique.<sup>34,35</sup> The first approach is quite feasible if one uses a CCD detector. But in the described FDT system, additional spectral resolution measurements would add too much acquisition time. The most appropriate way to improve the capabilities of such systems is to use high-frequency amplitude modulation of excitation light (at least 50 to 100 MHz) and synchronous detection. The problem that arises here is modulation of the Nd:YAG laser (or another laser suitable for excitation of RFPs) with high frequency. But the traditional amplitude modulation of such a laser with a Q-switch is limited by the 1- to 5-ns pulse width and the 10-kHz repetition rate

that is not suitable for precision phase measurements.

### Acknowledgments

This work was partly supported by the Russian Foundation for Basic Research (project numbers 50276, 07-02-01262, and 07-02-01146), and by the Science and Innovations Federal Russian Agency (project number 02.522.11.2002).

### Appendix

In this appendix we derive a formula for the solution of the underdetermined system of linear equations

$$Av = p,$$

$$A \in R^{M \times N}, \quad v \in R^N, \quad p \in R^M, \quad M < N,$$

$$A = \{a_{ij} \geq 0, i = \overline{1, M}, j = \overline{1, N}\}, \quad (6)$$

and

$$p = \{p_i \geq 0, i = \overline{1, M}\}$$

with the minimal Holder norm [Eq. (4)]. This problem can be formulated as follows:

$$\min_{(v_1, \dots, v_N)^T \in \Sigma} \left[ \sum_{j=1}^N (v_j^2 + \varepsilon)^{\xi/2} \right] \quad (7)$$

Here,  $\Sigma = \{v : Av = p\}$  is a solution set, and  $\varepsilon$  is a small positive number (usually  $10^{-6}$  to  $10^{-9}$ ). The presence of variable  $\varepsilon$  allows the differentiation of Eq. (4) for the case of  $\xi \leq 1$ . The estimation of the conditional extremum reduces to the estimation of the extremum of the Lagrange function:

$$F(v, \lambda) = \sum_{j=1}^N (v_j^2 + \varepsilon)^{\xi/2} + \lambda(Av - p),$$

where  $\lambda$  is a  $1 \times M$  vector. Partial derivatives are equated to zero:

$$\begin{cases} \frac{\partial F}{\partial v_j} = \xi v_j (v_j^2 + \varepsilon)^{\xi/2-1} + \sum_{i=1}^M \lambda_i a_{ij} = 0 \\ \frac{\partial F}{\partial \lambda_i} = \sum_{j=1}^N a_{ij} v_j - p_i = 0 \end{cases};$$

or in matrix form, we can write

$$\begin{cases} \xi D_\xi(v)v + A^T \lambda^T = 0 \\ Av = p \end{cases}, \quad (8)$$

where  $D_\xi(v) = \text{diag}[(v_j^2 + \varepsilon)^{\xi/2-1}]$  is a diagonal matrix. By extracting  $v$  and  $\lambda^T$  from Eq. (8),

$$v = -\frac{1}{\xi} D_\xi^{-1}(v) A^T \lambda^T$$

and

$$Av = -\frac{1}{\xi}AD_{\xi}^{-1}(v)A^T\lambda^T = p \Rightarrow \lambda^T = -\xi[AD_{\xi}^{-1}(v)A^T]^{-1}p,$$

one can obtain an equation for  $v$ :

$$v = D_{\xi}^{-1}(v)A^T[AD_{\xi}^{-1}(v)A^T]^{-1}p. \quad (9)$$

For the special case of  $\xi=2$  and  $D_2=E$ , Eq. (9) transforms into the well-known formula for evaluating a solution with the minimal Euclidean norm:

$$v = A^T(AA^T)^{-1}b. \quad (10)$$

The value of  $\xi$  can be set to 0, because matrix  $D_{\xi}(v)$  has no singularity at the point  $\xi=0$ . With this fact taken into account, Eq. (9) can be written in the following form:

$$v = D_0^{-1}(v)A^T[AD_0^{-1}(v)A^T]^{-1}p. \quad (11)$$

Equation (11) allows one to write the iteration process:

$$v^{(k+1)} = D_0^{-1}(v^{(k)})A^T[AD_0^{-1}[v^{(k)}]A^T]^{-1}p, \quad (12)$$

where  $v^{(0)}$  may be calculated from Eq. (10). The criterion for finishing the iteration procedure can be chosen as follows:

$$\frac{\|v^{(k+1)} - v^{(k)}\|_2^2}{\|v^{(k+1)}\|_2^2} \leq \delta_0^2.$$

Here,  $\delta_0$  is a small value (usually 0.01 to 0.1).

The algorithm based on the Holder norm converges to some solution, because the function of the iteration process (9) is a contracting mapping.

## References

- R. M. Hoffman, "Green fluorescent protein imaging of tumor cells in mice," *Lab Anim.* **31**, 34–41 (2002).
- M. H. Katz, S. Takimoto, D. Spivack, A. R. Moossa, R. M. Hoffman, and M. Bouvet, "A novel red fluorescent protein orthotopic pancreatic cancer model for the preclinical evaluation of chemotherapeutics," *J. Surg. Res.* **113**, 151–160 (2003).
- R. M. Hoffman and M. Yang, "Whole-body imaging with fluorescent proteins," *Nat. Protocol.* **1**(3), 1429–1438 (2006).
- R. M. Hoffman, "The multiple uses of fluorescent proteins to visualize cancer *in vivo*," *Nat. Rev. Cancer* **5**, 797–806 (2006).
- M. V. Matz, A. F. Fradkov, Y. A. Labas, A. P. Savitsky, A. G. Zaraisky, M. L. Markelov, and S. A. Lukyanov, "Fluorescent proteins from nonbioluminescent Anthozoa species," *Nat. Biotechnol.* **17**, 969–973 (1999).
- N. C. Shaner, P. A. Steinbach, and R. Y. Tsien, "A guide to choosing fluorescent proteins," *Nat. Methods* **2**(12), 905–909 (2005).
- A. A. Heikal, S. T. Hess, G. S. Baird, R. Y. Tsien, and W. W. Webb, "Molecular spectroscopy and dynamics of intrinsically fluorescent proteins: Coral red (dsRed) and yellow (citrine)," *Proc. Natl. Acad. Sci. U.S.A.* **97**(22), 11996–12001 (2000).
- M. A. O'Leary, D. A. Boas, X. D. Li, B. Chance, and A. G. Yodh, "Fluorescence lifetime imaging in turbid media," *Opt. Lett.* **21**, 158–160 (1996).
- M. S. Patterson, B. Chance, and B. C. Wilson, "Time resolved reflectance and transmittance for the noninvasive measurement of tissue optical properties," *Appl. Opt.* **28**, 2331–2336 (1989).
- V. Ntziachristos, J. Ripoll, L. V. Wang, and R. Weissleder, "Looking and listening to light: the evolution of whole-body photonic imaging," *Nat. Biotechnol.* **23**, 313–320 (2005).
- V. Ntziachristos and R. Weissleder, "Charge-coupled-device based scanner for tomography of fluorescent near-infrared probes in turbid media," *Med. Phys.* **29**, 803–809 (2000).
- A. Godavarty, M. J. Eppstein, Ch. Zhang, S. Theru, A. B. Thompson, M. Gurfinkel, and E. M. Sevick-Muraca, "Fluorescence-enhanced optical imaging in large tissue volumes using a gain-modulated ICCD camera," *Phys. Med. Biol.* **48**, 1701–1720 (2003).
- S. V. Patwardhan, S. R. Bloch, S. Achilefu, and J. P. Culver, "Time-dependent whole-body fluorescence tomography of probe biodistributions in mice," *Opt. Express* **13**(7), 2564–2577 (2005).
- V. Ntziachristos, Ch. Tung, Chr. Bremer, and R. Weissleder, "Fluorescence molecular tomography resolves protease activity *in vivo*," *Quantum Opt.* **8**, 757–760 (2002).
- A. Soubret and V. Ntziachristos, "Fluorescence molecular tomography in the presence of background fluorescence," *Phys. Med. Biol.* **51**, 3983–4001 (2006).
- S. Bloch, F. Lesage, L. McIntosh, A. Gandjbakhche, K. Liang, and S. Achilefu, "Whole-body fluorescence lifetime imaging of a tumor-targeted near-infrared molecular probe in mice," *J. Biomed. Opt.* **10**(5), 054003 (2005).
- G. Zacharakis, J. Ripoll, R. Weissleder, and V. Ntziachristos, "Fluorescent protein tomography scanner for small animal imaging," *IEEE Trans. Med. Imaging* **24**(7), 878–885 (2005).
- H. Meyer, A. Garofalakis, G. Zacharakis, S. Psycharakis, C. Marmalaki, D. Kioussis, E. N. Economou, V. Ntziachristos, and J. Ripoll, "Noncontact optical imaging in mice with full angular coverage and automatic surface extraction," *Appl. Opt.* **46**(17), 3617–3627 (2007).
- I. V. Turchin, V. I. Plehanov, A. G. Orlova, V. A. Kamensky, M. S. Kleshnin, M. V. Shirmanova, N. M. Shakhova, I. V. Balalaeva, and A. P. Savitsky, "Fluorescence diffuse tomography of small animals with DsRed2 fluorescent protein," *Laser Phys.* **3**(4), 208–211 (2006).
- G. Zacharakis, H. Shih, J. Ripoll, R. Weissleder, and V. Ntziachristos, "Normalized transillumination of fluorescent proteins in small animals," *Mol. Imaging* **5**(3), 153–159 (2006).
- A. Garofalakis, G. Zacharakis, H. Meyer, E. N. Economou, C. Marmalaki, J. Papamatheakis, D. Kioussis, V. Ntziachristos, and J. Ripoll, "Three-dimensional *in vivo* imaging of green fluorescent protein-expressing T cells in mice with noncontact fluorescence molecular tomography," *Mol. Imaging* **6**(2), 96–107 (2007).
- E. E. Graves, J. P. Culver, J. Ripoll, R. Weissleder, and V. Ntziachristos, "Singular-value analysis and optimization of experimental parameters in fluorescence molecular tomography," *J. Opt. Soc. Am. A* **21**(2), 231–241 (2004).
- X. Intes, V. Ntziachristos, J. P. Culver, A. Yodh, and B. Chance, "Projection access order in algebraic reconstruction technique for diffuse optical tomography," *Phys. Med. Biol.* **47**, N1–N10 (2002).
- V. V. Lyubimov, A. G. Kalintsev, A. B. Konovalov, O. V. Lyamtsev, O. V. Kravtchenyuk, A. G. Murzin, O. V. Golubkina, G. B. Mordvinov, L. N. Soms, and L. M. Yavorskaya, "Application of the photon average trajectories method to real-time reconstruction of tissue inhomogeneities in diffuse optical tomography of strongly scattering media," *Phys. Med. Biol.* **47**, 2109–2128 (2002).
- J. B. Fishkin and E. Gratton, "Propagation of photon-density waves in strongly scattering media containing an absorbing semi-infinite plane bounded by a straight edge," *J. Opt. Soc. Am. A* **10**(1), 127–140 (1993).
- A. Ishimaru, "Wave Propagation and Scattering in Random Media," v.1 "Single Scattering and Transport Theory," Academic Press, New York (1978).
- R. B. Schulz, J. Ripoll, and V. Ntziachristos, "Experimental fluorescence tomography of tissues with noncontact measurements," *IEEE Trans. Med. Imaging* **23**(4), 492–500 (2004).
- B. J. Bevis and B. S. Glick, "Rapidly maturing variants of the *Discosoma* red fluorescent protein (DsRed)," *Nat. Biotechnol.* **20**, 83–87 (2002).
- E. M. Merzlyak, J. Goedhart, D. Sherbo, M. E. Bulina, A. S. Shcheglov, A. F. Fradkov, A. Gaintzeva, K. A. Lukyanov, S. Lukyanov, T. W. J. Gadella, and D. M. Chudakov, "Bright monomeric red fluorescent protein with an extended fluorescence lifetime," *Nat. Methods* **4**, 555–557 (2007).
- L. C. Robinson and J. S. Marchant, "Improved 'optical highlighter' probes derived from *Discosoma* red fluorescent protein," *Biophys. J.* **88**, 1444–1457 (2005).
- D. Shcherbo, E. M. Merzlyak, T. V. Chepurnykh, A. F. Fradkov, G. V. Ermakova, E. A. Solovieva, K. A. Lukyanov, E. A. Bogdanova, A. G. Zaraisky, S. Lukyanov, and D. M. Chudakov, "Bright far-red fluorescent protein for whole-body imaging," *Nat. Methods* **4**(9), 741–746 (2007).

32. A. Soubret, J. Ripoll, and V. Ntziachristos, "Accuracy of fluorescent tomography in the presence of heterogeneities: Study of the normalized Born ratio," *IEEE Trans. Med. Imaging* **24**(10), 1377–1386 (2005).
33. J. R. Mansfield, K. W. Gossage, C. C. Hoyt, and R. M. Levenson, "Autofluorescence removal, multiplexing, and automated analysis methods for in-vivo fluorescence imaging," *J. Biomed. Opt.* **10**(4), 041207 (2005).
34. D. Y. Paithankar, A. U. Chen, B. W. Pogue, M. S. Patterson, and E. M. Sevick-Muraca, "Imaging of fluorescent yield and lifetime from multiply scattered light reemitted from random media," *Appl. Opt.* **36**(10), 2260–2272 (1997).
35. R. Roy, A. Godavarty, and E. M. Sevick-Muraca, "Fluorescence-enhanced three-dimensional lifetime imaging: a phantom study," *Phys. Med. Biol.* **52**, 4155–4170 (2007).